Single-Ion versus Dipolar Origin of the Magnetic Anisotropy in Iron(III)-Oxo Clusters: A Case Study

Gian Luca Abbati,[b] Louis-Claude Brunel,[c] Helene Casalta,[d] Andrea Cornia,[b] Antonio C. Fabretti,[b] Dante Gatteschi,*[a] Aia K. Hassan,[c] Aloysius G. M. Jansen,[e] Anna Lisa Maniero,[c] Luca Pardi,[f] Carley Paulsen,[g] and Ulderico Segre[b]

Abstract: A multitechnique approach has allowed the first experimental determination of single-ion anisotropies in a large iron(III)-oxo cluster, namely $[NaFe_6(OCH_3)_{12}(pmdbm)_6]ClO_4$ (**1**) in which Hpmdbm = 1,3-bis(4-methoxyphenyl)-1,3-propanedione. High-frequency EPR (HF-EPR), bulk susceptibility measurements, and high-field cantilever torque magnetometry (HF-CTM) have been applied to iron-doped samples of an isomorphous hexagallium(III) cluster $[NaGa_6(OCH_3)_{12}(pmdbm)_6]ClO_4$, whose synthesis and X-ray structure are also presented. HF-EPR at 240 GHz and susceptibility data have shown that the iron(III) ions have a hard-axis type anisotropy with $D^{Fe} = 0.43(1)\ cm^{-1}$ and $E^{Fe} = 0.066(3)\ cm^{-1}$ in the zero-field splitting (ZFS) Hamiltonian $\mathbf{H} = D^{Fe}[\mathbf{S}_z^2 - S(S+1)/3] + E^{Fe}[\mathbf{S}_x^2 - \mathbf{S}_y^2]$. HF-CTM at 0.4 K has then been used to establish the orientation of the ZFS tensors with respect to the unique molecular axis of the cluster, Z. The hard magnetic axes of the iron(III) ions are found to be almost perpendicular to Z, so that the anisotropic components projected onto Z are negative, $D^{Fe}(ZZ) = -0.164(4)\ cm^{-1}$. Due to the dominant antiferromagnetic coupling, a negative $D^{Fe}(ZZ)$ value determines a hard-axis molecular anisotropy in **1**, as experimentally observed. By adding point-dipolar interactions between iron(III) spins, the calculated ZFS parameter of the triplet state, $D_1 = 4.70(9)\ cm^{-1}$, is in excellent agreement with that determined by inelastic neutron scattering experiments at 2 K, $D_1 = 4.57(2)\ cm^{-1}$. Iron-doped samples of a structurally related compound, the dimer $[Ga_2(OCH_3)_2(dbm)_4]$ (Hdbm = dibenzoylmethane), have also been investigated by HF-EPR at 525 GHz. The single-ion anisotropy is of the hard-axis type as well, but the D^{Fe} parameter is significantly larger [$D^{Fe} = 0.770(3)\ cm^{-1}$, $E^{Fe} = 0.090(3)\ cm^{-1}$]. We conclude that, although the ZFS tensors depend very unpredictably on the coordination environment of the metal ions, single-ion terms can contribute significantly to the magnetic anisotropy of iron(III)-oxo clusters, which are currently investigated as single-molecule magnets.

Keywords: cluster compounds · EPR spectroscopy · gallium · iron · magnetic properties

Introduction

Magnetic anisotropy studies have proven to be an invaluable tool for investigating the electronic structure of transition metal and rare earth compounds.[1] However, the experimental determination of magnetic anisotropy has been a difficult problem and indeed accurate investigations of magnetic anisotropy are relatively rare. Things have begun to change in the last few years, because new much more powerful experimental techniques have become available, such as high-

[a] Prof. D. Gatteschi
Dipartimento di Chimica, Università degli Studi di Firenze
Via Maragliano 77, 50144 Firenze (Italy)
Fax: (+39) 055-354845
E-mail: gattesch@chim1.unifi.it

[b] Dr. G. L. Abbati, Dr. A. Cornia, Prof. A. C. Fabretti, Prof. U. Segre
Dipartimento di Chimica
Università degli Studi di Modena e Reggio Emilia
41100 Modena (Italy)

[c] Dr. L.-C. Brunel, Dr. A. K. Hassan, Dr. A. L. Maniero
National High Magnetic Field Laboratory
Tallahassee, Florida 32310 (USA)

[d] Dr. H. Casalta
Institut Laue Langevin
CNRS, 38042 Grenoble (France)

[e] Dr. A. G. M. Jansen
Grenoble High Magnetic Field Laboratory
MPI-FKF and CNRS, 38042 Grenoble (France)

[f] Dr. L. Pardi
Istituto di Fisica Atomica e Molecolare
CNR, 56127 Pisa (Italy)

[g] Dr. C. Paulsen
Centre de Recherches sur les Très Basses Temperatures
CNRS, 38042 Grenoble (France)

  0947-6539/01/0708-1796 $ 17.50+.50/0

field cantilever torque magnetometry (HF-CTM),[2] micro-SQUID arrays,[3] and high-frequency EPR (HF-EPR).[4] Further interest in magnetic anisotropy has increased with the development of molecular magnets; this requires deep understanding of magnetic anisotropy to control the properties of the new materials.[5] A clear example of the importance of magnetic anisotropy in molecular magnetism is provided by the so-called single-molecule magnets (SMM).[6] The SMM behavior was first discovered in a mixed-valence manganese cluster, $[Mn_{12}O_{12}(CH_3COO)_{16}(H_2O)_4]$ (Mn_{12}),[7] and subsequently in many other molecular clusters that contain iron,[8, 9] manganese,[10, 11] and vanadium ions.[12] It is characterized by an exceedingly slow paramagnetic relaxation at low temperature, with a relaxation time of the magnetization which is as long as two months in Mn_{12} at 2 K. As a result, these molecules have a magnetic hysteresis cycle similar to that observed in bulk magnets and can in principle be used for practical applications, like information storage at the molecular level or quantum computing. At the origin of the interesting behavior is a large easy-axis magnetic anisotropy and a large energy barrier that must be overcome for the reversal of the magnetic moment. The energy barrier is about 60 K in Mn_{12}, so that SMM behavior is observed only below liquid helium temperature. It is apparent that the synthesis of new molecular clusters which may behave as SMMs at higher temperatures would represent a tremendous breakthrough in this area. This proves to be a formidable task since it requires a strict control, at the synthetic level, of both the spin of the ground state and the magnetic anisotropy. Up to now, several clusters with a large S value (up to 51/2) have been assembled by a proper choice of the interacting metal ions and of the bridging ligands, but most of them are characterized by a highly symmetrical structure, which is expected to lead to a small ground-state zero-field splitting (ZFS) and, consequently, to a small energy barrier.[13] Hence, it is now becoming increasingly clear that any nonserendipitous progress in this area requires a more fundamental understanding of the origin and structural dependence of magnetic anisotropy.[4]

In many molecular clusters the anisotropy is magneto-crystalline in nature, that is, it is associated with the ZFS of the total spin states. In the case of strongly anisotropic metal ions, like Jahn–Teller distorted high-spin manganese(III) ($S=2$), single-ion terms are likely to provide a leading contribution to magnetic anisotropy.[14] It is now generally accepted that the large Ising-type anisotropy of Mn_{12} is indeed due to the single-ion contribution.[6b, 11g,h] In the case of weakly-anisotropic metal ions, like high-spin iron(III) ($S=5/2$), the situation becomes more complicated because single-ion and dipolar contributions are expected to have a comparable magnitude.[4, 8, 9a] In principle, additional terms arising from exchange anisotropy are expected, although they should be small due to the essentially isotropic g factor of the iron(III) ions. Since an increasing number of iron(III)-oxo clusters have SMM behavior,[8] we have undertaken an extensive experimental study on the origin of magnetic anisotropy in a model iron(III) cluster, $[NaFe_6(OCH_3)_{12}(pmdbm)_6]ClO_4$ (**1**), in which Hpmdbm = 1,3-bis(4-methoxyphenyl)-1,3-propanedione. This compound has an $S=0$ ground state and was chosen for its particularly appealing molecular structure, which contains six crystallographically equivalent iron(III) ions.[15] The first-excited triplet state ($S=1$) becomes the ground state in the presence of strong magnetic fields and its ZFS parameter has been experimentally determined.[16] The dipolar interaction alone is not enough to justify the observed ZFS, suggesting that single-ion contributions may be important. On the other hand, in other antiferromagnetic rings the ZFS of the excited spin multiplets with $S>0$ has been shown to be almost perfectly justified by dipolar interactions alone.[16] Therefore a deeper understanding of the factors affecting the single-ion contribution to the magnetic anisotropy in iron(III) ions is needed.

In order to obtain direct information on the single-ion iron(III) anisotropy it is necessary to have the metal ions magnetically isolated in an environment which is as similar as possible to that of the iron in the magnetic cluster. The strategy we followed was that of synthesizing a diamagnetic hexagallium(III) cluster, $[NaGa_6(OCH_3)_{12}(pmdbm)_6]ClO_4$ (**2**), which is isomorphous to **1**, and a dinuclear compound $[Ga_2(OCH_3)_2(dbm)_4]$ (**3**) (Hdbm = dibenzoylmethane). At low iron(III) doping content isolated paramagnetic ions in a diamagnetic host are present, and the single-ion anisotropy

Abstract in Italian: *Le anisotropie magnetiche di singolo ione in un cluster di ferro(III)-oxo ad elevata nuclearità, $[NaFe_6(OCH_3)_{12}(pmdbm)_6]ClO_4$ (**1**) dove Hpmdbm = 1,3-bis(4-metossifenil)-1,3-propandione, sono state determinate sperimentalmente per la prima volta. Spettri EPR ad Alta Frequenza (HF-EPR), misure di suscettività e di momento torcente in campi elevati (HF-CTM) sono stati eseguiti su un cluster isomorfo di gallio(III) drogato con ioni ferro(III), $[NaGa_6(OCH_3)_{12}(pmdbm)_6]ClO_4$, di cui riportiamo la sintesi e la struttura ai raggi-X. I dati HF-EPR a 240 GHz e le misure di suscettività hanno rivelato un'anisotropia di tipo hard-axis per gli ioni ferro(III), con $D^{Fe}=0.43(1)\ cm^{-1}$ e $E^{Fe}=0.066(3)$ nell'hamiltoniano di zero-field splitting (ZFS) $\boldsymbol{H}=D^{Fe}[\boldsymbol{S}_z^2 - S(S+1)/3] + E^{Fe}[\boldsymbol{S}_x^2 - \boldsymbol{S}_y^2]$. Le misure di HF-CTM a 0.4 K hanno permesso di determinare l'orientazione dei tensori di ZFS rispetto all'asse unico del cluster, Z. Gli assi z degli ioni ferro(III) sono diretti pressochè perpendicolarmente a Z cosicchè le componenti di ZFS proiettate lungo Z sono negative, $D^{Fe}(ZZ)=-0.164(4)\ cm^{-1}$. A causa delle interazioni antiferromagnetiche tra centri metallici, il segno negativo di $D^{Fe}(ZZ)$ determina un'anisotropia molecolare di tipo hard-axis in **1**, come osservato sperimentalmente. Il parametro di ZFS per lo stato di tripletto, $D_1=4.70(9)\ cm^{-1}$, calcolato aggiungendo i contributi dipolari ai termini di singolo ione, risulta in eccellente accordo con il valore misurato mediante lo Scattering Inelastico di Neutroni a 2 K, $D_1=4.57(2)\ cm^{-1}$. Le anisotropie di singolo ione possono dunque contribuire in modo significativo all'anisotropia magnetica dei nanomagneti molecolari a base di cluster ferro(III)-oxo. I tensori di ZFS sono tuttavia alquanto sensibili a piccole differenze nell'intorno di coordinazione degli ioni ferro(III), come mostrano studi HF-EPR a 525 GHz su campioni drogati del dimero $[Ga_2(OCH_3)_2(dbm)_4]$ [Hdbm = dibenzoilmetano, $D^{Fe}=0.770(3)\ cm^{-1}$, $E^{Fe}=0.090(3)\ cm^{-1}$].*

can be directly measured by using HF-EPR, bulk susceptibility measurements, and HF-CTM on single crystals. The experimental strategy herein presented, combined with the results of inelastic neutron scattering (INS) experiments on the magnetic hexairon(III) compound **1**, has provided for the first time a complete picture of the different anisotropic contributions in a large iron(III)-oxo cluster, and we wish to present it here as a case study.

Results and Discussion

Synthesis: The reaction of transition metal salts with alkali metal alkoxides and β-diketones has been extensively used for assembling large magnetic clusters.[17] The alkali-metal salt is typically a Li, Na, or K methoxide and often plays a crucial role in the synthesis. On one hand, the alkoxide ligands are very effective in promoting the aggregation of the metal-oxo core, which is held together by bridging RO^- groups. On the other hand, the alkali-metal cation may drive the core formation by acting as a template.[17a,b] This subtle effect is apparent in the case of ringlike clusters such as $[NaFe_6(OCH_3)_{12}(pmdbm)_6]ClO_4$ (**1**)[15, 17c] and the isostructural manganese(III) species,[17d] which invariably encapsulate an Li or Na ion. In this work, we have used this synthetic technique to prepare taylor-made di- and hexagallium(III) clusters isostructural to iron(III) compounds previously reported.[15, 18] The synthesis of $[NaGa_6(OCH_3)_{12}(pmdbm)_6]ClO_4$ (**2**) and $[Ga_2(OCH_3)_2(dbm)_4]$ (**3**) was accomplished by reacting anhydrous gallium(III) chloride with stoichiometric amounts of Hpmdbm or Hdbm and an alkali-metal methoxide in anhydrous methanol [see Eqs. (1) and (2)]. This procedure led to extensive precipitation of a white flocculent solid, which could be recrystallized from chloroform/methanol mixtures. Considerably less soluble precipitates were obtained by using reagent-grade methanol, probably due to the partial formation of gallium(III)-oxohydroxides.

$$6\,GaCl_3 + 6\,Hpmdbm + 18\,NaOCH_3 + NaClO_4 \longrightarrow [NaGa_6(OCH_3)_{12}(pmdbm)_6]ClO_4\ (\mathbf{2}) + 6\,CH_3OH + 18\,NaCl \quad (1)$$

$$2\,GaCl_3 + 4\,Hdbm + 6\,NaOCH_3 \longrightarrow [Ga_2(OCH_3)_2(dbm)_4]\ (\mathbf{3}) + 4\,CH_3OH + 6\,NaCl \quad (2)$$

Dry crystals of **2** undergo rapid solvent loss. Furthermore, in the solid state **2** is very sensitive to moisture even in the presence of the mother liquid, but it can be stored unaltered for several months in a sealed vessel at 5 °C. By contrast, the crystals of **3**, like those of the isomorphous iron(III) complex $[Fe_2(OCH_3)_2(dbm)_4]$ (**4**),[18] are air stable.

Iron(III)-doped samples of both di- and hexagallium(III) clusters were prepared by using a mixture of gallium(III) and iron(III) chlorides in the synthesis. The optimal Fe/Ga molar ratio (p) was determined by modelling isomorphic substitutions as independent events, so that the mole fraction of the $Ga_{n-m}Fe_m$ species (P_{nm} with n and m integer) follows binomial distribution [Eq. (3)]

$$P_{nm} = \frac{n!}{m!(n-m)!}\, p^m (1-p)^{n-m} \quad (3)$$

In Figure 1 we plot the mole fraction of mono- ($= P_{n1}$) and polysubstituted ($= 1 - P_{n0} - P_{n1}$) species for $n = 2$ (dimer) and 6 (hexamer). The values $p = 0.1$ (for $n = 2$) and 0.02 (for $n = 6$) were chosen so as to have $P_{n1}/(1 - P_{n0} - P_{n1}) \sim 20$, that is, a high ratio between mono- and polysubstituted clusters. Notice that under these conditions about 10 and 20 % of the clusters, respectively, are magnetic as they contain *at least* one iron ion.

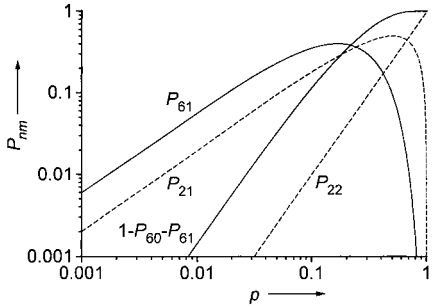

Figure 1. Mole fraction of mono- (P_{n1}) and polysubstituted ($1 - P_{n0} - P_{n1}$) species for the doped dimer ($n = 2$) and hexamer ($n = 6$) as a function of the Fe/Ga molar ratio, p.

Crystal structures: Complexes **2** and **3** form colorless molecular crystals that are isomorphous to those of the corresponding iron(III) compounds. Accurate unit cell parameters and other experimental details are reported in Table 1. The

Table 1. Crystallographic data for compounds **2** and **3**.

	2	**3**
formula	$C_{120}H_{132}Ga_6O_{40}NaCl_{19}$[a]	$C_{62}H_{50}Ga_2O_{10}$
M_r	3329.12[a]	1094.46
crystal system	trigonal	triclinic
space group[b]	$R\bar{3}$	$P\bar{1}$
a [Å]	28.073(4)	9.6251(8)
b [Å]	28.073(4)	10.8800(10)
c [Å]	16.402(4)	12.9930(10)
α [°]	90	79.980(10)
β [°]	90	87.856(8)
γ [°]	120	82.470(9)
V [Å^3]	11195(4)	1328.2(2)
Z	3	1
T [K]	223(2)	293(2)
ρ_{calcd} [g cm^{-3}]	1.48[a]	1.37
μ [cm^{-1}]	14.84[a]	10.74
transmission (min/max)	0.76/0.87	0.75/0.76
$2\theta_{max}$ [°]	48.0	55.0
radiation	$Mo_{K\alpha}$	$Mo_{K\alpha}$
λ [Å]	0.71069	0.71069
scan mode	ω-2θ	ω-2θ
reflections collected	6321	6339
independent reflections	3815	6069
observed reflections [$I > 2\sigma(I)$]	2643	3597
parameters	366	434
min./max. residues [e Å^{-3}]	−0.78/0.80	−0.31/0.29
$R1(F_o)$[c]	0.0639	0.0418
$wR2(F_o^2)$[d]	0.1697[e]	0.1030[f]
GOF[g]	1.029	0.947

[a] With $x = 6$, $y = 0$. [b] Ref. [40]. [c] On independent reflections with $I > 2\sigma(I)$; $R1 = \Sigma||F_o| - |F_c||/\Sigma|F_o|$. [d] On all data; $wR2 = [\Sigma w(F_o^2 - F_c^2)^2/\Sigma w(F_o)^4]^{1/2}$. [e] $w = 1/[\sigma^2(F_o^2) + (0.0859P)^2 + (38.8746P)]$ and $P = [\max(F_o^2, 0) + 2F_c^2]/3$. [f] $w = 1/[\sigma^2(F_o^2) + (0.0433P)^2]$; see footnote [e] for a definition of P. [g] $GOF = [\Sigma w(F_o^2 - F_c^2)^2/(n-p)]^{1/2}$, where n is the number of reflections used for refinement and p is the total number of parameters refined.

0947-6539/01/0708-1798 $ 17.50+.50/0 *Chem. Eur. J.* **2001**, *7*, No. 8

hexagallium(III) cation in **2** (Figure 2) is virtually identical to **1**, with the six crystallographically equivalent gallium(III) ions defining an essentially coplanar ring (deviation: 0.0734(7) Å).[15] The molecule has sixfold symmetry due to the presence of a crystallographic S_6 axis passing through the central sodium atom and perpendicular to the average molecular plane. Selected geometric parameters of **1** and **2** are compared in Table 2. Both the distance between nearest-neighboring metal ions and the ring size, defined as the $M\cdots M^c$ separation, are smaller in the gallium(III) compound by 0.0736(9) Å and 0.147(1) Å, respectively. Noticeably, the $M\cdots M^a\cdots M^b$ angles are identical in the two cases. Corresponding M–O bond lengths are also invariably smaller in **2** by 0.02 – 0.04 Å, while O-M-O and M-O-M angles deviate by less than 2.1° in the two species, with the exception of O4-M-O3 which is significantly more acute in **1** than in **2** (85.8(1)° vs 89.77(16)°). The above described structural differences are evidently associated with the smaller ionic radius of gallium(III) with respect to high-spin iron(III) (0.62 vs 0.64 Å).

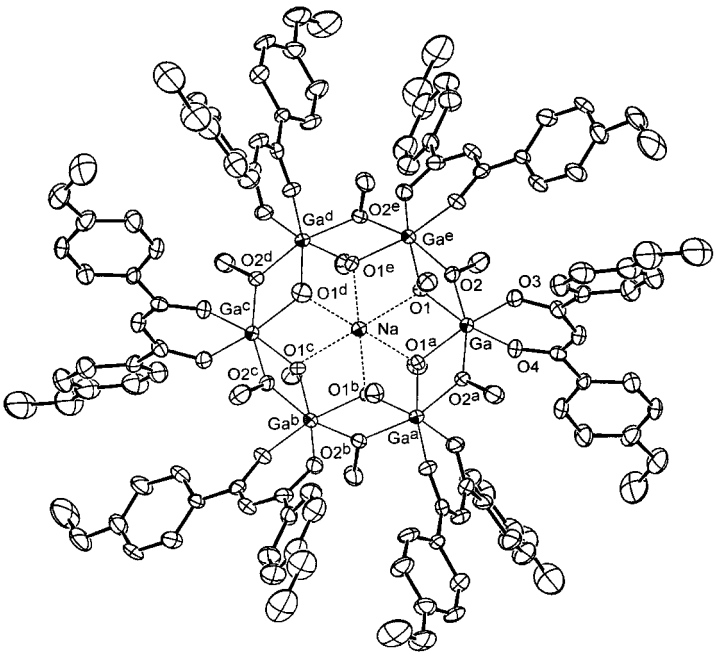

Figure 2. Molecular structure of the hexagallium(III) cation in **2**. Hydrogen atoms are omitted for clarity.

Table 2. Selected interatomic distances [Å] and angles [°] for **1** and **2**.[a]

	1 (M = Fe)	**2** (M = Ga)
$M\cdots M^a$	3.2152(5)	3.1416(7)
$M\cdots M^b$	5.5627(9)	5.435(13)
$M\cdots M^c$	6.425(1)	6.278(14)
M–O1	2.023(3)	1.980(4)
$M–O1^a$	2.041(3)	2.019(4)
M–O2	2.000(4)	1.971(4)
$M–O2^a$	2.014(3)	1.973(4)
M–O3	2.001(3)	1.966(4)
M–O4	1.982(3)	1.956(4)
Na–O1	2.352(1)	2.290(4)
$M\cdots M^a\cdots M^b$	119.781(4)	119.782(4)
O2-M-O1	74.8(1)	75.85(15)
$O2^a$-M-$O1^a$	74.1(1)	74.91(15)
O3-M-O1	89.0(1)	87.28(16)
O4-M-$O1^a$	93.8(2)	91.73(15)
O3-M-O2	101.6(2)	100.68(16)
O4-M-O2	94.4(1)	93.94(16)
O4-M-O3	85.8(1)	89.77(16)
$O2^a$-M-O1	97.2(2)	96.29(16)
O2-M-$O1^a$	90.9(1)	90.62(15)
O3-M-$O2^a$	93.4(2)	93.58(16)
O4-M-$O2^a$	95.2(2)	94.85(16)
O1-M-$O1^a$	93.8(2)	93.4(2)
O4-M-O1	166.8(1)	168.63(16)
O3-M-$O1^a$	167.4(1)	168.48(16)
O2-M-$O2^a$	162.7(2)	163.26(19)
O1-Na-$O1^a$	78.2(1)	78.88(12)
O1-Na-$O1^b$	101.8(1)	101.11(12)
M-$O1^a$-M^a	104.6(2)	103.55(17)
M-$O2^a$-M^a	106.5(2)	105.61(18)

[a] Superscripts are used for symmetry-equivalent atoms [$X^a = S_6^1$ (X), $X^b = S_6^2$ (X), etc.].

The molecular structure of the digallium(III) complex **3** (Figure 3) is centrosymmetric and identical to that observed in the iron(III) compound (**4**).[18] Selected geometric parameters of **3** and **4** are compared in Table 3. The $M\cdots M'$ separation is smaller in the gallium complex by 0.074(12) Å, while the average M–O bond length decreases from 1.997(13) Å in **4** to 1.957(17) Å in **3**. The M-O1-M angles are equal to each other within experimental error.

To our knowledge, the six-membered cyclic structure of **2** is unprecedented among oxo-bridged gallium(III) clusters. These include the trimeric μ_3-oxo-centered carboxylate $[Ga_3(O)(O_2CPh)_6(4\text{-Me-py})_3]^+$,[19a] the tetranuclear complex $[Ga_4(OH)_6(3\text{-}t\text{Bu-Hpz})_{10}]^{6+}$ with a "butterfly" core,[19b] and the octagallium(III) cluster $[Ga_8(pz)_{12}O_4Cl_4]$ (Hpz = pyrazole).[20] In the latter, four penta-coordinated gallium(III) ions are connected to an inner Ga_4O_4 cubane core through μ_4-oxo and pyrazolato bridges.

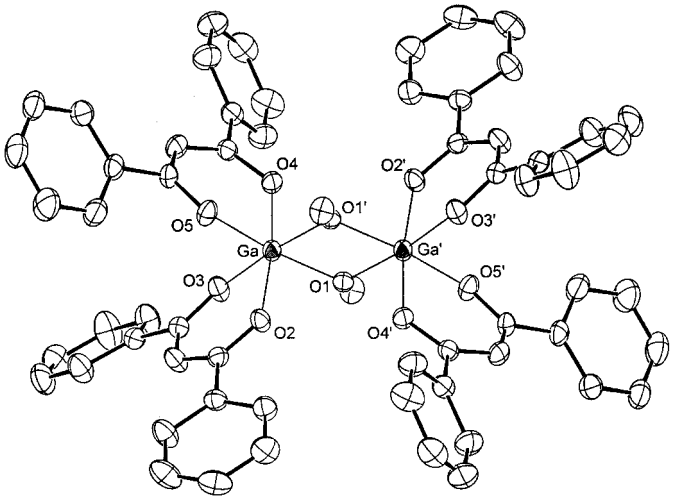

Figure 3. Molecular structure of the digallium(III) complex **3**. Hydrogen atoms are omitted for clarity.

By contrast, the $\{Ga_2O_2\}$ core of **3** is a recurrent structural motif in gallium coordination chemistry and has been observed in various hydroxo-,[21a,b] alkoxo-,[21c–f] and alkylperoxo-bridged[21g] complexes. The metal can be either in a tetrahedral[21c,f,g] or octahedral[21a,b,d,e] coordination environment. The Ga-O1-Ga′ and O1′-Ga-O1 angles observed in **3**

Table 3. Selected interatomic distances [Å] and angles [°] for **3** and **4**.[a]

	3 (M = Ga)	**4** (M = Fe)
M···M′	3.0132(7)	3.087(1)
M-O1	1.9309(19)	1.978(3)
M-O1′	1.9482(19)	1.995(3)
M-O2	1.9677(19)	2.007(4)
M-O3	1.978(2)	2.007(4)
M-O4	1.9683(18)	2.007(3)
M-O5	1.950(2)	1.986(4)
M′-O1-M	101.93(9)	102.0(2)
O4-M-O1	91.63(8)	90.8(1)
O4-M-O1′	97.33(8)	100.8(1)
O4-M-O5	89.21(8)	86.5(1)
O4-M-O2	171.96(8)	168.7(1)
O3-M-O1	95.79(9)	95.8(2)
O5-M-O3	92.98(9)	93.5(2)
O1′-M-O2	89.87(8)	89.2(1)
O1′-M-O1	78.07(9)	80.0(2)
O5-M-O1	171.24(8)	170.1(2)
O2-M-O1	93.36(8)	96.5(1)
O5-M-O2	86.82(9)	87.7(2)
O3-M-O4	84.47(8)	85.2(2)
O3-M-O2	88.76(8)	85.5(1)
O1′-M-O5	93.17(8)	93.1(1)
O1′-M-O3	173.61(8)	171.4(2)

[a] Primed atoms are related to unprimed ones by an inversion center.

(101.93(9) and 78.07(9)° respectively, see Table 3) are equal, within experimental error, to those reported for $[Ga_2(OR)_2(tBu)_2]$[21c] (101.7(1) and 78.3(1)° respectively, R = *t*Bu or Ph) and $[Ga_2(OCH_3)_2(ang)_2]$[21d] (101.6(3) and 78.4(3)° respectively, H_2ang = anguibactin); this points to a remarkable insensitivity of the geometry of the $\{Ga_2O_2\}$ ring with respect to the coordination number of the metal (four and six, respectively).

DC-SQUID magnetic measurements: Microcrystalline samples of $[NaGa_{6-z}Fe_z(OCH_3)_{12}(pmdbm)_6]ClO_4$ (**2-doped**) were characterized by magnetization measurements at 2.8–20 K with applied fields in the range 0.3–4.0 T. The susceptibility data are reported in Figure 4 as a function of temperature for

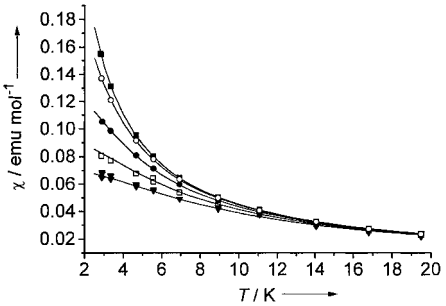

Figure 4. Magnetic susceptibility of **2-doped** as a function of temperature at 0.3 T (■), 1.0 T (○), 2.0 T (●), 3.0 T (□) and 4.0 T (▼). The best-fit curves are also shown (see text for details).

five different magnetic field values. The χT product at 20 K (ca. 0.45 emu K mol^{-1}) is only a small fraction of that expected for an isolated $S = 5/2$ spin (4.38 emu K mol^{-1} with $g = 2.00$). As shown by the solid curves, the magnetic susceptibility data can be nicely reproduced assuming 0.1002(3) mol of isolated $S = 5/2$ spins per mole of cluster. The resulting iron content (0.17 % w/w) is identical to that determined by elemental analysis. Also, a 0.0167 mole fraction of Fe atoms is calculated which is very close to that used in the synthesis (0.02). These data confirm that the iron(III) ions are well diluted in the diamagnetic matrix and indicate that, neglecting polysubstituted species, about 10 % of the clusters contain one iron atom. Additional magnetic measurements in the temperature range 0.27–6.9 K were performed in order to attempt a first-hand estimate of single-ion anisotropies. The data collected with an applied field of 0.0255 T are reported in Figure 5 as a

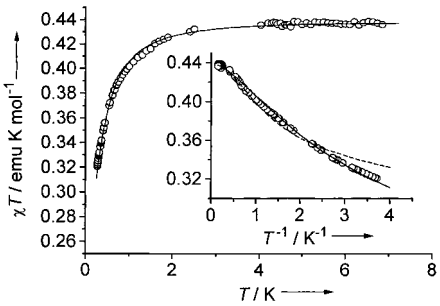

Figure 5. χT product of **2-doped** as a function of temperature at 0.0255 T. The inset shows a χT versus $1/T$ plot. Calculated curves for $D^{Fe} = 0.45$ cm^{-1} (solid) and $D^{Fe} = -0.42$ cm^{-1} (dashed), which provide the best fit to the experimetal χT versus T data, are also shown.

χT versus T plot. Due to the very low applied field, the smooth decrease of the χT product at the lowest temperatures cannot be due to saturation effects, but rather to ZFS of the $S = 5/2$ state. ZFS effects were modeled by using a second-order spin Hamiltonian, given in general form by Equation (4):

$$\mathbf{H} = \mu_B \mathbf{S}\cdot\mathbf{g}\cdot\mathbf{B} + D^{Fe}[\mathbf{S}_z^2 - S(S+1)/3] + E^{Fe}[\mathbf{S}_x^2 - \mathbf{S}_y^2] \quad (4)$$

In Equation (4), the axes of the local coordinate frame *xyz* (lower case) are chosen along the principal directions of the iron(III) ZFS tensor. For the sake of simplicity, in the analysis of susceptibility measurements we assumed axial symmetry ($E^{Fe} = 0$) and an isotropic $g = 2.00$, and we treated D^{Fe} and an overall scale factor as adjustable parameters. The experimental data provide strong evidence for a hard-axis anisotropy, with $D^{Fe} = 0.42(2)$ cm^{-1}. The reported uncertainty of the D^{Fe} value mainly reflects the slightly different results obtained by using different fitting procedures (for instance, fitting χ or χT). A negative D^{Fe} parameter invariably yielded a much worse fit, especially in the low-temperature region, as can be clearly appreciated by plotting χT against $1/T$ (inset in Figure 5).

High-frequency EPR (HF-EPR) spectra: A more detailed investigation of single-ion anisotropies in **2-doped** was based on HF-EPR spectroscopy. HF-EPR represents an unrivaled technique for investigating the ZFS in paramagnetic transition metal complexes, with recent outstanding results in the field of high-spin molecules.[4, 9a, 10a,b,g,h, 11f] Compared to magnetometry techniques it provides information on the local environment of the metal ions, rather than a crystal average. For an $S = 5/2$ with an axial ZFS ($E^{Fe}/D^{Fe} = 0$) ten allowed transitions are expected, while for a rhombic system ($E^{Fe}/D^{Fe} \neq 0$) fifteen transitions are predicted. In a powder

0947-6539/01/0708-1800 $ 17.50+.50/0 *Chem. Eur. J.* **2001**, *7*, No. 8

spectrum the features observed are those relative to the allowed transitions along the ZFS principal axes (x, y, z) and the out-of-axis turning points, for which the magnetic field lies within a principal plane. In Figure 6 we report the spectra

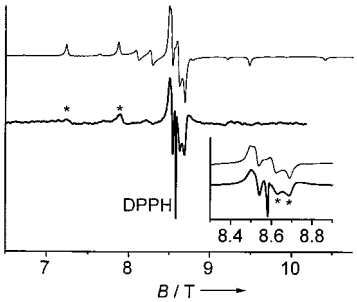

Figure 6. Experimental (bold curve) and calculated (standard curve) HF-EPR spectrum of **2-doped** at 240 GHz and 15 K. The sharp signal in the experimental spectrum is due to DPPH (DPPH = 2,2-diphenyl-1-picrylhydrazyl). The region around $g = 2$ is shown in more detail in the inset.

recorded on a microcrystalline sample of **2-doped** at 240 GHz and 15 K. At this frequency, the free-electron resonance ($g = 2.0023$) is observed at about 8.56 T, as shown by the sharp DPPH signal. The spectrum is dominated by a multiplet centered at 8.6 T, with weaker resonances at 7.24 and 7.90 T (marked with an asterisk) and, possibly, very weak bands at about 8.22 and 9.20 T. The resonance pattern at $g \sim 2$ (see Figure 6, inset) is typical for the $M_S = +1/2 \rightleftharpoons -1/2$ transitions of a half-integer spin system with $S > 1/2$ and moderate rhombic distortion. In the case of chromium(III)-doped $YAlO_3$, for instance, the z, x, and y components of the $M_S = +1/2 \rightleftharpoons -1/2$ transition are observed around $g = 2$, while two characteristic off-axis lines appear at higher magnetic field values.[22] The strong peaks at 8.62 and 8.69 T (marked with an asterisk in the inset of Figure 6) are most probably due to off-axis resonances. For a quantitative analysis of the spectra, we observed that the lines at 7.24, 7.90, and 9.22 T and the $g = 2$ resonance are evenly spaced in magnetic field by $\Delta B = 0.66$ T, as typically observed for "canonical" peaks of the z, x, and y components of ZFS. In the limit of a dominant Zeeman term, as is usually the case with HF-EPR, the field spacing $\Delta B_{x,y,z}$ is related to the D^{Fe} and E^{Fe} parameters by the Equations (5a)–(5c):

$$g\mu_B \Delta B_x = D^{Fe} - 3E^{Fe} \quad (5a)$$

$$g\mu_B \Delta B_y = D^{Fe} + 3E^{Fe} \quad (5b)$$

$$g\mu_B \Delta B_z = 2D^{Fe} \quad (5c)$$

Assuming $g = 2.003$ and $D^{Fe} = 0.42$ cm^{-1}, as determined by susceptibility measurements, the observed line pattern must be assigned to the x or y components of ZFS, since a larger spacing would be expected for z transitions ($\Delta B_z = 0.90$ cm^{-1}). Consequently, the absolute value of the rhombic ZFS parameter is $|E^{Fe}| = (g\mu_B \Delta B - D^{Fe})/3 = 0.066$ cm^{-1}. Notice that the actual sign of E^{Fe} depends on the particular assignment of the observed resonances to x or y transitions and cannot be determined from powder spectra. Numerical simulation of the spectra in the parameter range $D^{Fe} = 0.3$–0.6 cm^{-1} and $0 \le E^{Fe}/D^{Fe} \le 1/3$ confirmed these conclusions, yielding $D^{Fe} = 0.43(1)$ cm^{-1} and $E^{Fe} = 0.066(3)$ as best-fit parameters with isotropic $g = 2.003$. Notice that the multiplet at $g \sim 2$ is nicely reproduced, as shown in Figure 6 (inset). However, it is apparent that the z and x components of the transitions other than $M_S = +1/2 \rightleftharpoons -1/2$ cannot be resolved in the spectra. Since the trigonal crystal axis is an easy magnetic direction (see next section), the intensity of the z and x lines is presumably reduced beyond detection by partial orientation of the crystallites in the applied magnetic field. Furthermore, the modulation of ZFS parameters arising from strain effects is known to provide a broadening mechanism for the EPR lines lying at the extremes of the spectrum.[4]

The HF-EPR spectra of $[Ga_{2-z}Fe_z(OCH_3)_2(dbm)_4]$ (**3-doped**) at 525 GHz and two different temperatures are shown in Figure 7. The spectra are typical of a high-spin ferric ion in

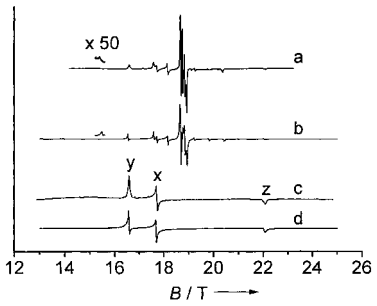

Figure 7. HF-EPR spectra of **3-doped** at 525 GHz and different temperatures. a) and c) are the experimental spectra at 30 K and 5 K respectively, while b) and d) are the corresponding calculated spectra (see text).

octahedral environment with dominant ZFS. The experimental 30 K spectrum shown in Figure 7a displays at least 15 transitions; this indicates that the E^{Fe}/D^{Fe} ratio must be different from zero. The low-temperature spectrum, shown in Figure 7c, shows three signals coming from the transition between the ground multiplet and the first excited state along the three principal directions of the ZFS as labeled in Figure 7c. The observed spectra were successfully simulated using the spin Hamiltonian in Equation (4) with the following parameters: $D^{Fe} = 0.770(3)$ cm^{-1}, $E^{Fe} = 0.090(3)$, $g_{\parallel} = 2.000$ and $g_{\perp} = 2.003$. The calculated spectra at 30 K and 5 K are reported in Figure 7b and 7d, respectively. The location of the transitions in the field is quite well reproduced although some of the features have a linewidth that is not satisfactorily reproduced. As already pointed out above this can be due to an incomplete model of the linewidth anisotropy or to the effect of higher order terms in the Hamiltonian.

The axial ZFS parameters in **2-doped** and **3-doped** are located above the upper limit in the series made up of octahedral ferric complexes with a FeO_6 chromophore.[23] In Table 4 we collect the results of EPR investigations on octahedral complexes with β-diketonate ligands, including **2-doped** and **3-doped**. Tris-diketonate complexes have smaller D^{Fe} values and larger rhombic distortions with respect to the remaining compounds. The iron(III) ions in both **2-doped** and

Table 4. Spin Hamiltonian parameters in some high-spin iron(III) complexes.

	D^{Fe} [cm^{-1}]	$\lvert E^{Fe}\rvert$ [cm^{-1}]	$\lvert E^{Fe}/D^{Fe}\rvert$	Ref.
$[Fe(acac)_3]$[a]	± 0.16	0.048	0.30	[41]
$[Fe(dpm)_3]$[b]	-0.18	0.045	0.25	[9a]
2-doped	0.43(1)	0.066(3)	0.15	this work
3-doped	0.770(3)	0.090(3)	0.12	this work

[a] Hacac = acetylacetone. [b] Hdpm = dipivaloylmethane.

3-doped have a positive D^{Fe}, with a larger rhombic component in the former compound.

High-field cantilever torque magnetometry (HF-CTM): Additional experiments on single crystals were performed by HF-CTM in fields up to 10 T. This technique has been recently used to investigate the electronic structure of large magnetic clusters, such as Mn_{12}[2a,b] and ringlike antiferromagnets.[16, 24] We show herein that the exceedingly high sensitivity of this macroscopic technique allows us to investigate magnetically diluted samples as well. CTM measures the magnetic torque $\mathbf{t} = \mathbf{M} \times \mathbf{B}$, which acts on a magnetically-anisotropic sample in a homogeneous magnetic field **B** (**M** is the magnetization of the sample). Cantilevers are usually sensitive to one component of the torque vector only, that is, that responsible for cantilever flexion. In the experimental setup of Figure 8, for

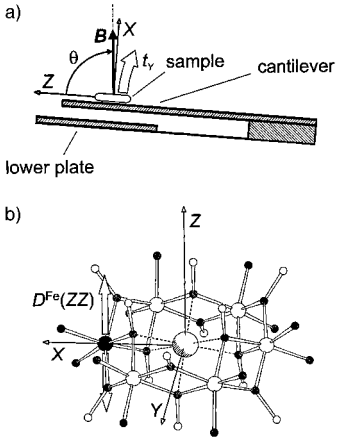

Figure 8. a) Experimental setup used in the torque experiments, with the crystal coordinate frame *XYZ*. The device measures the *Y* component of the torque (t_Y). The θ angle can be varied by rotating the torquemeter around *Y*. b) View of a Ga_5Fe molecule in **2-doped**. The coordinate system *XYZ* has the *Z* direction along the trigonal molecular axis, and the *X* and *Y* axes arbitrarily directed in the molecular plane. Atom: large empty spheres = Ga, black sphere = Fe, shaded sphere = Na, small hatched spheres = O, small empty spheres = C. Hydrogen atoms and pmdbm ligands are omitted for clarity.

instance, cantilever deflection is due to t_Y and provides information on the magnetic anisotropy in the *XZ* plane. Notice that upper-case *XYZ* denotes the crystal coordinate system, while lower-case *xyz* is used for the local coordinate frame of the iron(III) ions [see Eq. (4)]. In capacitive torquemeters, magnetic torque is actually measured from the capacitance change ($\Delta C = C_0 - C_B$) of the device upon application of the magnetic field.

Due to the low iron content and to the very small size of the crystals, we assembled an array of about 80 individual crystals with collinear unique axes (within 5°), but disordered azimuthal angles. The sample size turned out to be sufficient to obtain an excellent signal-to-noise ratio. In Figure 9 we plot

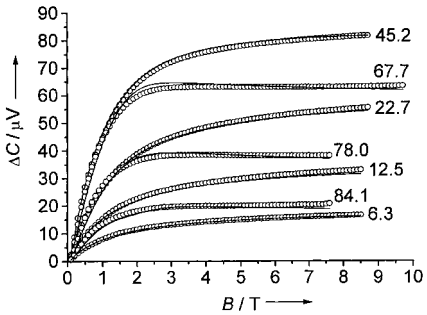

Figure 9. Torque data recorded on **2-doped** at 0.38(1) K for different θ angles as a function of applied field. Each curve is labelled with the corresponding θ value. Best-fit curves are also shown (see text for details).

ΔC against B curves recorded at 0.38(1) K for different sample orientations, as described by the angle θ between the magnetic field and the unique crystal axis, *Z* (Figure 8a). For all the explored θ values, the signal increases rapidly with increasing field and approaches a saturation value in high fields, as expected for a paramagnetic substance in a homogeneous magnetic field.[16b] Furthermore, the signal intensity is strongly modulated by the sample orientation. More precisely, the torque signal has a maximum for $\theta = 45°$ and vanishes for $\theta = 0°$ or 90°, that is, when the magnetic field is directed along one of the principal crystallographic directions. The sign of ΔC can be immediately used to distinguish between an easy-axis or a hard-axis magnetic anisotropy. Since we found $\Delta C > 0$ (i.e. $C_B < C_0$), it follows from Figure 8a that the sample tends to rotate so as to bring the sixfold cluster axis along the applied magnetic field. Consequently, the trigonal axis (*Z*) is an easy magnetic direction in the doped single crystal; this means that the dopant iron(III) ions must have negative ZFS components along *Z*. We now turn to a quantitative analysis of torque data by first examining the low-field region in Figure 9. For an axial easy-axis paramagnet a low-field peak is expected in the t_Y against B curves at $\theta \sim 90°$, as recently observed in Mn_{12}.[2a] Similarly, for a hard-axis paramagnet a torque peak should be present at $\theta \sim 0°$. A qualitatively similar behavior is predicted in the presence of rhombic distortion provided that the magnetic field is applied perpendicular to an easy direction in the *XZ* plane. The set of experimental curves in Figure 9 shows no peak in the torque signal for θ close to 0° or 90°. As will be shown hereafter, this feature is closely related to averaging effects and can be exploited to determine the orientation of the local fine-structure tensors. In fact due to the sixfold crystal symmetry the iron dopant will be evenly distributed among the six equivalent sites, so that the magnetic response of each doped crystal will be determined by six overlapping contributions. Furthermore, the completely disordered azimuthal angles of the crystals in the sample introduce additional averaging effects over a macroscopic

0947-6539/01/0708-1802 $ 17.50+.50/0 *Chem. Eur. J.* **2001**, *7*, No. 8

scale. Both effects can be accounted for by considering an ensemble of anisotropic $S = 5/2$ paramagnets with the same D^{Fe}, E^{fe}, and g values but different orientation of the ZFS tensor, as described by the Eulerian angles α, β, and γ.[25] These angles are defined in Figure 10. As usual, α and β

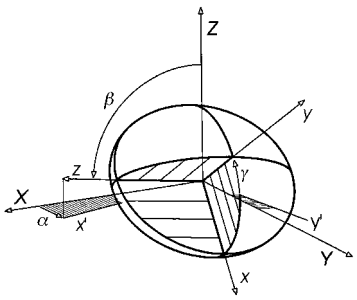

Figure 10. Eulerian angles used to describe the orientation of the ZFS-tensor. The x' and y' axes lie in the XY plane. Notice that xyz (lower case) denotes the local coordinate frame of the iron(III) ions, while XYZ (upper case) is the fixed crystal frame.

correspond to the polar angles of the z axis in the fixed coordinate frame XYZ. The γ angle, which is relevant only for $E^{Fe} \neq 0$, describes the rotation of the ZFS tensor around the local z axis and determines the orientation of the principal axes in the plane perpendicular to z (for $\gamma = 0$ the y axis lies in the XY plane). Since Z is chosen along the sixfold molecular axis, the sample can be modeled by an ensemble of paramagnets related by a arbitrary rotation around Z, that is, with identical β and γ angles, but a different α angle. In general, the low-temperature torque response of the ensemble differs substantially from that of an isolated paramagnet and depends strongly upon the angles β and γ. We used this simple model to simultaneously fit the seven torque curves reported in Figure 9. The θ angle for each curve was fixed at the setting value used in the torque experiments. However, an overall scale factor for the torque signal was refined, since an accurate weighing of the sample was unpracticable. The D^{Fe} and E^{Fe} parameters were fixed at the values determined by HF-EPR (0.43(1) and 0.066(3) cm^{-1}, respectively), while the Eulerian angles β and γ were treated as adjustable parameters. The best-fit angles obtained from this procedure are $\beta = 79.2(4)^\circ$ and $\gamma = 62(2)^\circ$.

Inelastic neutron scattering (INS) spectra: Together with HF-EPR, INS represents a leading technique for magnetic anisotropy investigations in molecular clusters.[24, 26, 27] In Figure 11, we plot the neutron-scattering intensity recorded at 2 K as a function of energy transfer on a microcrystalline sample of **1**. Under these conditions, only the fundamental $S = 0$ level is populated and one can observe energy loss transitions of the neutron. Two peaks are observed at $\Delta\varepsilon_1 = 1.520(2)$ meV and $\Delta\varepsilon_2 = 2.087(1)$ meV (1 meV ~ 8.065 cm^{-1}) which can be described by a gaussian of the same width as the resolution (see Experimental Section). The second peak presents a very broad feature on the low-energy side for which we have no explanation yet. As shown by previous work on ring-like antiferromagnets, in which the T and Q dependence of the spectra was also investigated,[24] the two

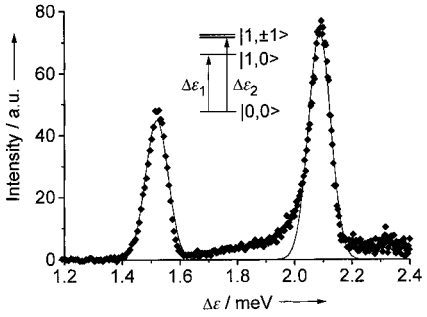

Figure 11. Inelastic neutron scattering intensity as a function of energy transfer as recorded on compound **1** at 2 K. The inset shows the transitions which are responsible for the observed absorptions.

peaks can be assigned to the transitions from the ground state $|0,0\rangle$ to the split levels $|1,0\rangle$ and $|1,\pm1\rangle$ of the first excited triplet state. The triplet-singlet energy gap and the axial ZFS of the triplet state are thus easily determined as $E_1 = (1/3)\Delta\varepsilon_1 + (2/3)\Delta\varepsilon_2 = 15.31(1)$ and $D_1 = \Delta\varepsilon_2 - \Delta\varepsilon_1 = 4.57(2)$ cm^{-1}, respectively. The same parameters previously determined by HF-CTM at 0.45 K are $E_1 = 15.28(1)$ and $D_1 = 4.32(2)$ cm^{-1}.[16a] Considering that INS directly probes the zero-field spectrum of spin levels, while HF-CTM does not, the agreement between the two sets of spin Hamiltonian parameters can be regarded as satisfactory.

The origin of the magnetic anisotropy: In principle, the spin structure of the clusters in the absence of applied magnetic fields can be described by using the spin Hamiltonian in Equation (6):

$$\mathbf{H} = \mathbf{H}^{iso} + \mathbf{H}^{anis} \quad (6)$$

where $\mathbf{H}^{anis}$ is defined as in Equation (7):

$$\mathbf{H}^{anis} = \mathbf{H}^{Fe} + \mathbf{H}^{ex} + \mathbf{H}^{dip} \quad (7)$$

$\mathbf{H}^{iso}$ and $\mathbf{H}^{anis}$ represent the isotropic and anisotropic components of the spin Hamiltonian, respectively. The isotropic term, $\mathbf{H}^{iso}$, is associated with exchange-coupling interactions between spins and usually provides the leading contribution to Equation (6). The anisotropic term $\mathbf{H}^{anis}$ is composed of three different contributions that reflect single-ion anisotropies ($\mathbf{H}^{Fe}$) and the anisotropic components of spin–spin interactions. The latter can be either exchange ($\mathbf{H}^{ex}$) or dipolar ($\mathbf{H}^{dip}$) in nature. In principle, antisymmetric exchange terms and hyperfine (or superhyperfine) interactions with magnetic nuclei should be included in the Hamiltonian. The former vanish when the structure is centrosymmetric, as in **1**.[28] The latter can be neglected as far as static magnetic properties are concerned, although their influence on the spin dynamics has been recently pointed out.[29]

According to Equation (7), the $\mathbf{D}$ tensor of the triplet state in **1** ($\mathbf{D}_1$) can be considered as a sum of three different terms that reflect single-ion, dipolar, and exchange contributions [Eq. (8)].

$$\mathbf{D}_1 = \mathbf{D}_1^{Fe} + \mathbf{D}_1^{dip} + \mathbf{D}_1^{ex} \quad (8)$$

Notice that all the tensors appearing in Equation (8) must be axial and collinear owing to the symmetry of the crystal lattice. As a consequence, one can replace each tensor with the corresponding axial ZFS parameter, hereafter denoted as D_1, D_1^{Fe}, D_1^{dip}, and D_1^{ex}. At the simplest level of approximation, the dipolar term can be calculated by using the point-dipole model, which yields $D_1^{dip} = 1.16\ cm^{-1}$.[16] The positive sign of D_1^{dip} is typical for planar clusters with dominant antiferromagnetic coupling. In fact, dipolar energy is minimized when the spins lie perpendicular to the molecular plane, and this arrangement determines a hard-axis contribution to magnetic anisotropy.[8] Thus, dipolar interactions contribute significantly to the observed ZFS in **1**, although they do *not* represent the leading anisotropic term. Turning now to single-ion contributions, the $\mathbf{D}_1^{Fe}$ term in Equation (8) can be written as a linear combination of the six iron(III) fine-structure tensors, $\mathbf{D}^{Fe(i)}$ [Eq. (9)]:[28]

$$\mathbf{D}_1^{Fe} = \sum_{i=1}^{6} c_1^i \mathbf{D}^{Fe(i)} \quad (9)$$

Because the six iron(III) ions are equivalent, the projection coefficients c_1^i must be identical to each other. They can be evaluated from a detailed knowledge of the spin functions for the system ($c_1^i = -12/5$).[15, 24, 28] The most important consequence of Equation (9) is that D_1^{Fe} is determined only by the ZZ component of the single-ion tensors, $D^{Fe}(ZZ)$ (see Figure 8b), as given by Equation (10):

$$D_1^{Fe} = \tfrac{3}{2} D_1^{Fe}(ZZ) = \tfrac{3}{2} \sum_{i=1}^{6} c_1^i D^{Fe}(ZZ) = -\tfrac{108}{5} D^{Fe}(ZZ) \quad (10)$$

$D^{Fe}(ZZ)$ can also be expressed as a function of the Eulerian angles β and γ [Eq. (11)]:

$$D^{Fe}(ZZ) = D^{Fe}(\cos^2\beta - \tfrac{1}{3}) + E^{Fe}\sin^2\beta\cos 2\gamma \quad (11)$$

Hence, for a given set of D^{Fe} and E^{Fe} values, the D_1^{Fe} parameter depends critically on the orientation of the $\mathbf{D}^{Fe(i)}$ tensors with respect to the unique molecular axis Z. Previous treatments have been largely based on the assumption of axial and collinear $\mathbf{D}^{Fe(i)}$ tensors ($\beta = 0$), as suggested by the trigonal distortion of the coordination environments along the cluster axis.[15, 24] By contrast, the Eulerian angles obtained by HF-CTM, $\beta = 79.2(4)^\circ$ and $\gamma = 62(2)^\circ$, indicate that the hard magnetic axes of the six iron(III) ions are almost perpendicular to Z. Hence the assumption of collinear tensors is completely unrealistic for **1**. Furthermore, although the D^{Fe} parameters of the individual ions are positive, negative ZFS components are projected along the molecular axis owing to the large β value. The ZZ component calculated by using Equation (11) is $D^{Fe}(ZZ) = -0.164(4)\ cm^{-1}$, so that $D_1^{Fe} = 3.54(9)\ cm^{-1}$ from Equation (10). By neglecting exchange anisotropy in Equation (8) we finally find $D_1 \cong D_1^{Fe} + D_1^{dip} = 4.70(9)\ cm^{-1}$. The latter value is within 1.5σ from that determined by INS at 2 K.

Our experimental approach proves that single-ion ZFS contributions *plus* magnetic interactions between point dipoles localized on the metal centers account for virtually 100% of the observed molecular anisotropy in **1**. Both terms contribute to the observed hard-axis anisotropy of **1**, although single-ion ZFS dominates and is responsible for about 75% of the triplet ZFS. Apparently, the additional terms arising from exchange anisotropy and the corrections to the point-dipolar model are either negligible or, less likely, cancel each other out exactly.

Finally, we notice that the $D^{Fe}(ZZ)$ component is invariant upon rotation of the $\mathbf{D}^{Fe(k)}$ tensor around the Z axis, so that the Eulerian α angles of the individual tensors cannot be determined from experiment (although $\alpha_k = \alpha_1 + (k-1)4\pi/3$ by symmetry). Theoretical calculations are needed to clarify which features of the coordination environment dictate the sign and magnitude of single-ion anisotropy in high-spin iron(III) complexes. Recent work by Neese and Solomon[30] has shown that subtle electronic effects, like anisotropic covalency, charge-transfer states, and ligand spin-orbit coupling, play a crucial role in determining the ZFS parameters. These effects are clearly out of reach for simple ligand-field approaches, like the angular overlap model,[9a, 14, 31] which are indeed unable to account for the large ZFS parameters observed in **2-doped** and **3-doped**.[32]

Conclusion

Our experiments on **2-doped** were designed so as to obtain an independent determination of single-ion contributions to the magnetic anisotropy of a large iron(III)-oxo cluster. A two-step approach was devised to obtain information on the ZFS parameters of the single ions and on the orientation of the local anisotropy tensors with respect to the ring axis. The first step was based on low-field magnetic susceptibility measurements and HF-EPR spectra on powder samples. These techniques are known to provide a local measurement of single-ion properties and, as a consequence, they can be used to determine the diagonal elements of the ZFS tensors ($\mathbf{D}^{Fe(i)}$), but not the orientation of the principal axes with respect to the crystal axes. The second step was based on torque magnetometry in high magnetic field, a technique which has been recently used to investigate spin crossover in **1** and in similar molecular antiferromagnets. HF-CTM was used in a highly complementary approach to obtain the orientation of the $\mathbf{D}^{Fe(i)}$ tensors with respect to the unique cluster axis. Notice that the sixfold symmetry of the cluster greatly facilitates this kind of analysis, because the six $\mathbf{D}^{Fe(i)}$ tensors are all equivalent, although not necessarily collinear. It is important to notice that the single-ion contribution obtained from the dinuclear species is remarkably different from that for the hexanuclear species. If the D^{Fe} value determined for the dinuclear species were used for calculating the ZFS of **1**, the agreement between calculated and experimental values would have been much less satisfactory. More sophisticated approaches, like density functional theory or Hartree–Fock calculations, should be employed in order to reach a deeper understanding of which structural parameters should be modified in order to produce the expected magnetic anisotropy.[30] We plan to work in this area in the near future. However, a clear indication that emerges from this work is that the experimental apparatus for accurately measuring magnetic anisotropy is now available, and it should be widely used by all the groups interested in the characterization of paramagnetic species.

0947-6539/01/0708-1804 $ 17.50+.50/0 *Chem. Eur. J.* **2001**, *7*, No. 8

Experimental Section

Analytical procedures: Analytical determinations were carried out on microcrystalline samples of all the compounds. C, H elemental analysis was performed by using a Carlo Erba EA1110 CHNS-O automatic analyzer. Metal-content determinations were carried out with an inductively coupled plasma (ICP) spectrometer SPECTRO D after decomposition of the sample in a Kjeldahl flask with a sulfo-nitric acid mixture, followed by treatment with a concentrated hydrogen peroxide solution.[33a] The samples for chlorine determination were decomposed by alkaline fusion with sodium peroxide.[33b] Chlorine was titrated potentiometrically as chloride ion with a silver nitrate solution by using an AMEL titrimetric apparatus (mod. 233 digital burette and mod. 234 titrator) interfaced with a Omni-Scribe recorder.

Synthetic procedures: All operations were carried out with strict exclusion of moisture, unless otherwise stated. Gallium(III) trichloride (Aldrich, 99.99%), iron wire (Carlo Erba, 99.99%), sublimed iron(III) chloride (Carlo Erba, 99%), sodium perchlorate (Carlo Erba), dibenzoylmethane (Avocado), sodium metal, sodium methylate, and lithium methylate (Fluka) were used as received. Chloroform (Fluka) was distilled from $CaCl_2$ shortly before use, while reagent-grade methanol (Fluka) was carefully dried by treatment with Mg/I_2 and distilled.[34] Hpmdbm was synthesized as described elsewhere[15] and recrystallized from hot ethanol before use. $[NaFe_6(OCH_3)_{12}(pmdbm)_6]ClO_4$ (**1**) was prepared as previously reported.[15] Gallium(III) trichloride (5.23 g) was carefully dissolved in methanol (250.0 mL) to give a 0.119 M stock solution. *Attention! $GaCl_3$ reacts violently with methanol.* A 0.60 M methanolic solution of $NaOCH_3$ was freshly prepared from sodium metal and methanol. The use of sublimed $FeCl_3$ as an iron source to synthesize **2-doped** and **3-doped** proved to be satisfactory for the doped dimer only. Preliminary HF-EPR spectra of **2-doped** prepared by using $FeCl_3$ showed the characteristic six-lines hyperfine pattern of ^{55}Mn ($I = 5/2$) around $g = 2$. For this reason, a 0.0217 M solution of iron(III) chloride was prepared by dissolving iron wire (0.0121 g) in a few drops of HCl/HNO_3. The solution was evaporated to dryness and the residue was redissolved in the minimum amount of HCl (37%). Methanol was then added to reach a 10.0 mL volume.

$[NaGa_6(OCH_3)_{12}(pmdbm)_6]ClO_4 \cdot x CHCl_3 \cdot y CH_3OH$ (2): Hpmdbm (0.568 g, 2 mmol) dissolved in methanol (33.0 mL) was added to the $GaCl_3$ stock solution (16.8 mL, 2 mmol). After 15 minutes stirring, the sodium methoxide solution (10.0 mL, 6 mmol) was added dropwise with vigorous stirring to give a white precipitate. The mixture was stirred for 10 minutes, then a few more drops of the sodium methoxide solution were added until precipitation was complete. Chloroform (60.0 mL) was then added to give a slightly cloudy solution, which was saturated with $NaClO_4$. Some undissolved material was separated by centrifugation and 2/3 of the solvent was slowly evaporated by gentle vacuum-pumping in a desiccator over P_2O_5 (60 mmHg, 7–9 hours). Finally, the flask was sealed and stored at 5 °C. Upon standing overnight, a white microcrystalline solid was obtained in ca. 50% yield. The precipitate was collected by filtration and dried under vacuum (15 min, 0.2 mm Hg). Elemental analysis calcd (%) for $C_{127.4}H_{163.4}Ga_6O_{48}NaCl_{17.2}$ ($x = 5.4$, $y = 8$; 3514.0): C 43.55, H 4.69, Cl 17.35, Na 0.66; found C 43.22, H 4.20, Cl 16.74, Na 0.70.

$[Ga_2(OCH_3)_2(dbm)_4]$ (3): Solid $GaCl_3$ (0.176 g, 1 mmol) was dissolved in methanol (10.0 mL). A solution of Hdbm (0.449 g, 2 mmol) and sodium methoxide (0.162 g, 3 mmol) in methanol (15.0 mL) was added dropwise with stirring. At the end of the addition, the white precipitate was collected by filtration and dissolved in chloroform (40.0 mL). The solution was layered with an equal amount of methanol. Colorless air-stable crystals formed in 1–2 days. Elemental analysis calcd (%) for $C_{62}H_{50}Ga_2O_{10}$ (1094.5): C 68.04, H 4.60; found: C 68.05, H 5.05.

$[NaGa_{6-z}Fe_z(OCH_3)_{12}(pmdbm)_6]ClO_4 \cdot x CHCl_3 \cdot y CH_3OH$ (2-doped): Hpmdbm (0.568 g, 2 mmol) was added to the sodium methoxide solution (20.0 mL, 6 mmol). The stock solutions of gallium(III) chloride (16.5 mL, 1.96 mmol) and iron(III) chloride (1.85 mL, 0.04 mmol) were mixed. The β-diketonate solution was added dropwise with stirring, whereupon the mixture progressively turned to dark green and then reddish-brown. At about half of the addition, a light pink precipitate started to appear. After the addition was complete, the suspension was stirred for further 30 minutes, then chloroform (80.0 mL) was added to give a bright orange solution. The latter was saturated with $NaClO_4$, centrifuged to remove some undissolved material, and concentrated to 1/2 of the initial volume by gentle vacuum pumping. The flask was then sealed and stocked at 5 °C for two days. The bright orange microcrystalline solid obtained was collected by filtration and fluxed for 30 minutes with argon. Elemental analysis calcd (%) for $C_{122.5}H_{145}Ga_{5.9}Fe_{0.1}O_{43.5}NaCl_{16}$ ($x = 5$, $y = 3.5$, $z = 0.1$; 3320.6): C 44.31, H 4.40, Cl 17.08, Fe 0.17; found: C 44.44, H 4.41, Cl 17.56, Fe 0.17. The possible presence of chloride as counterion was excluded by potentiometric titration of an acetone solution of the cluster with aqueous silver nitrate.

$[Ga_{2-z}Fe_z(OCH_3)_2(dbm)_4]$ (3-doped): Hdbm (1.220 g, 5.44 mmol) and lithium methylate (0.305 g, 8.03 mmol) dissolved in methanol (50.0 mL) were added dropwise over a 45 min period to a solution of $GaCl_3$ (0.424 g, 2.41 mmol) and $FeCl_3$ (0.044 g, 0.27 mmol, 10% mol) in methanol (9.5 mL). A dark red color quickly appeared, progressively turning to orange as the addition went on. After the addition was complete, the mixture was stirred for three hours, and the pink-orange precipitate was collected by filtration and washed with methanol. Recrystallization by liquid diffusion of methanol in a chloroform solution of the compound gave air-stable orange crystals. Elemental analysis calcd (%) for $C_{62}H_{50}Ga_{1.8}Fe_{0.2}O_{10}$ ($z = 0.2$; 1091.7), C 68.21, H 4.62, Fe 1.02; found: C 68.23, H 4.62, Fe 1.05.

X-ray structure determinations: Compounds **2** and **3** crystallize in the form of colorless prisms. The selected crystal of **2** ($0.20 \times 0.12 \times 0.10$ mm) was extracted from the solution under a cold nitrogen gas stream and mounted on the top of a quartz fiber with a small amount of vacuum grease. The tip was quickly transferred to a Siemens P4/RA diffractometer equipped with a LT2A low-temperature apparatus working at 223(2) K. The selected crystal of **3** ($0.24 \times 0.12 \times 0.15$ mm) was glued with epoxy resin on the top of a thin quartz fiber and transferred to an Enraf Nonius CAD-4 four-circle diffractometer working at room temperature. The symmetry of the reciprocal lattice in **2** and **3** was found to be consistent with Laue classes $\bar{3}$ and $\bar{1}$, respectively. The systematic absences of **2** indicated $R3$ (no. 146) and $R\bar{3}$ (no. 148) as possible space groups. Intensity data were collected by using graphite-monochromated $Mo_{K\alpha}$ radiation and were corrected for absorption (empirical) and Lp effects. The two crystal structures were solved by direct methods with the SIR-97 program package,[35] which gave the positions of all non-hydrogen atoms in the clusters. Atom coordinates were found to be fully consistent with the centrosymmetric space groups $R\bar{3}$ (no. 148) and $P\bar{1}$ (no. 2) for compounds **2** and **3**, respectively. Structure refinement was carried out on F^2 by full-matrix least-squares techniques with SHELX-97[36] program. All hydrogen atoms in the clusters were located in ΔF maps, with the exception of three methyl hydrogens of *p*-OCH_3 substituents in **2**. These were added at calculated positions assuming an idealized bond geometry and C–H distances of 0.98 Å. Six disordered $CHCl_3$ molecules per cluster were located in the crystal lattice of **2**, but the position of the perchlorate anion could not be determined. All non-hydrogen atoms in the structures were treated anisotropically. Hydrogen atoms in **2** were assigned $B(H) = 1.5\,B_{eq}(C)$ and $1.2\,B_{eq}(C)$ for aliphatic and aromatic/methine carbon atoms, respectively. Isotropic thermal parameters were refined for all the hydrogen atoms in **3**. Crystallographic data (excluding structure factors) for the structures reported in this paper have been deposited with the Cambridge Crystallographic Data Centre as supplementary publication no. CCDC-150130 (**2**) and CCDC-150131 (**3**). Copies of the data can be obtained free of charge on application to CCDC, 12 Union Road, Cambridge CB2 1EZ, UK (Fax: (+44) 1223-336033; E-mail: deposit@ccdc.cam.ac.uk).

DC-SQUID magnetic measurements: DC susceptibility data on **2-doped** in the temperature range 2.8–20 K were obtained by using a Metronique MS02 SQUID magnetometer, with applied fields of 0.3, 1.0, 2.0, 3.0, and 4.0 T. Additional measurements from 0.27 to 6.9 K were performed in a magnetic field of 0.0255 T by using a low-temperature high-field SQUID magnetometer developed at the Centre des Recherches sur les Très Basses Temperatures in Grenoble (France). Magnetization versus field curves were found to be linear up to at least 0.05 T at the lowest temperature. Raw data typically taken on 10–15 mg samples were reduced by assuming a molecular weight of 3320.6, as indicated by elemental analysis. Corrections for the sample holder contribution and for molecular diamagnetism (-1766×10^{-6} emu mol^{-1} from Pascal's constants) were also applied.

High-frequency EPR (HF-EPR) spectra: Powder HF-EPR spectra of **2-doped** were recorded on three different spectrometers in the 110 to 525 GHz range of frequencies. At the National High Magnetic Field Laboratory in Tallahassee two HF-EPR spectrometers were used, namely

the one with a superconducting magnet (NHMFL1) described elsewere,[37a] which offers frequencies in the range from 110 to 550 GHz, and the spectrometer based on the use of the resistive Keck magnet for the 525 GHz spectra (NHMFL2). Details concerning this spectrometer can be found elsewhere.[37b] The reported 240 GHz spectra on **2-doped** were recorded at the HF-EPR facility in Pisa.[37c] The powders were ground in presence of the mother liquid, pressed in a pellet at about 2 $Mg\,cm^{-3}$, and cooled in zero magnetic field. Using this procedure we minimized the loss of solvent from the microcrystals and orientation phenomena. The HF-EPR spectra of **3-doped** were performed on powdered samples at the NHMFL1 and NHMFL2 spectrometers. The loose powder was finely ground and the resulting sample was transferred in a Teflon cup and frozen to liquid nitrogen in zero magnetic field.

High-field cantilever torque magnetometry (HF-CTM): Torque experiments were performed at the High Magnetic Field Laboratory in Grenoble (France) by using a one-leg Cu/Be cantilever (spoon diameter: 2.5 mm; leg length: 3 mm; leg width: 0.3 mm; thickness: 50 μm) combined with a 50 μm spacer. The capacitance of the torquemeter was measured as $\Delta C = C_0 - C_B$, where $C_0 = 1.12$ pF is the zero-field capacitance. The sensitivity of the phase-sensitive detection of capacitance variation was 8.72 $\mu V\,fF^{-1}$ for the used excitation (5 kHz). The signal was integrated with a time constant $\sim$1 s and sampled every 2 s. Temperature was measured by using a calibrated RuO resistor and was kept constant at 0.38 ± 0.01 K. About 80 microcrystals of **2-doped**, showing a well-developed trigonal axis and average dimensions $0.08 \times 0.08 \times 0.16$ mm, were chosen by using an optical stereomicroscope. They were aligned on a $1.5 \times 1.8 \times 0.1$ mm glass plate and covered with the minimum amount of Fomblin® perfluorinated grease (Ausimont). The latter was very effective in preventing solvent loss during room-temperature operations. The glass slide was then mounted on the cantilever surface with the unique crystal axis Z perpendicular to the rotation axis of the goniometer. The magnetic field (0–10 T) was applied by using a superconducting magnet (T02) with constant field-sweep rate $\pm 0.0108\ T\,s^{-1}$. Upfield and downfield runs performed at each torquemeter orientation revealed no hysteresis effects. The maximum signal measured corresponded to less than 1% of the zero-field capacitance, so that a linear cantilever response $\Delta C \propto t_Y$ was assumed throughout.[2a]

Inelastic neutron scattering (INS) spectra: INS measurements were performed with the high-energy-resolution time-of-flight spectrometer IN5 at the Institut Laue-Langevin in Grenoble (France) with an incident wavelenght of 5 Å. The experimental resolution at zero energy transfer was well described by a gaussian with a full-width-at-half-maximum of 0.093 meV as determined on a vanadium standard sample. Both samples were placed in a He cryostat and measured at 2 K for an energy transfer $\Delta\varepsilon = \varepsilon_i - \varepsilon_f$ ranging from -1.98 to 2.44 meV. ε_i and ε_f represent the initial and the final energy of the neutron, respectively, so that the energy transfer is defined to be negative when energy is lost by the sample. No scattering-angle dependence of the detected transitions was observed. Hence, we summed up the energy spectrum over all the detector positions to increase the counting statistics.

Computational details: HF-EPR spectra were analyzed with the aid of the programs SIM and SIMSPC kindly provided by H. Weihe.[38] The torque curves recorded on **2-doped** were fitted by considering an ensemble of identical $S = 5/2$ paramagnets whose ZFS-tensors are related by an arbitrary rotation (α) around the molecular Z axis. Each paramagnet was defined by the Eulerian angles α, β, and γ, which describe the coordinate rotation from XYZ to the "local frame", xyz, whose axes are taken along the principal directions of the ZFS-tensor (see Figure 10). Magnetization and torque were computed by diagonalizing the 6×6 matrix representative of Equation (4) on the $|5/2,M_S>$ basis ($M_S = -5/2$ to $+5/2$) and were integrated over about 50 α values. The NAG Fortran Library Routine E04FCF[39a] was used for data fitting, while matrix diagonalization was performed by using the ZHEEV routine (LAPACK Linear Algebra Package).[39b] Major calculations were carried out on a Digital Alpha 3000/800S computer.

Acknowledgement

This work was financially supported by the University of Modena and Reggio Emilia, by Italian MURST and CNR (PFMSTAII), and by the Networks 3MD and MOLNANOMAG under contract numbers ERB FMRX-CT98-0181 and HPRN CT-1999-00012, respectively. We thank Dr. A. Caneschi (Dipartimento di Chimica, Università degli Studi di Firenze) and Prof. W. Malavasi (Dipartimento di Chimica, Università degli Studi di Modena e Reggio Emilia) for assistance in magnetic susceptibility measurements and sample preparation, respectively.

[1] a) R. L. Carlin, *Magnetochemistry*, Springer, Berlin, **1986**, p. 317; b) W. De W. Horrocks, Jr., D. De W. Hall, *Coord. Chem. Rev.* **1971**, *6*, 147; c) S. Mitra, *Prog. Inorg. Chem.* **1977**, *22*, 309.

[2] a) A. Cornia, M. Affronte, A. G. M. Jansen, D. Gatteschi, A. Caneschi, R. Sessoli, *Chem. Phys. Lett.* **2000**, *322*, 477; b) J. A. A. Perenboom, J. S. Brooks, S. Hill, T. Hathaway, N. S. Dalal, *Phys. Rev. B* **1998**, *58*, 330; c) M. J. Naughton, J. P. Ulmet, A. Narjis, S. Askenazy, M. V. Chaparala, A. P. Hope, *Rev. Sci. Instrum.* **1997**, *68*, 4061.

[3] a) W. Wernsdorfer, R. Sessoli, *Science* **1999**, *284*, 133; b) W. Wernsdorfer, T. Ohm, C. Sangregorio, R. Sessoli, D. Mailly, C. Paulsen, *Phys. Rev. Lett.* **1999**, *82*, 3903.

[4] A. L. Barra, D. Gatteschi, R. Sessoli, *Chem. Eur. J.* **2000**, *6*, 1608.

[5] a) O. Kahn, *Molecular Magnetism*, VCH, Weinheim, **1993**; b) "Magnetic Molecular Materials": *NATO ASI Ser. E* **1991**, *198*.

[6] a) G. Aromi, S. M. J. Aubin, M. A. Bolcar, G. Christou, H. J. Eppley, K. Folting, D. N. Hendrickson, J. C. Huffman, R. C. Squire, H.-L. Tsai, S. Wang, M. W. Wemple, *Polyhedron* **1998**, *17*, 3005; b) S. M. J. Aubin, Z. M. Sun, I. A. Guzei, A. L. Rheingold, G. Christou, D. N. Hendrickson, *Chem. Commun.* **1997**, 2239.

[7] R. Sessoli, D. Gatteschi, A. Caneschi, M. A. Novak, *Nature* **1993**, *365*, 141.

[8] D. Gatteschi, R. Sessoli, A. Cornia, *Chem. Commun.* **2000**, 725.

[9] a) A. L. Barra, A. Caneschi, A. Cornia, F. Fabrizi de Biani, D. Gatteschi, C. Sangregorio, R. Sessoli, L. Sorace, *J. Am. Chem. Soc.* **1999**, *121*, 5302; b) J. C. Goodwin, R. Sessoli, D. Gatteschi, W. Wernsdorfer, A. K. Powell, S. L. Heath, *J. Chem. Soc. Dalton Trans.* **2000**, 1835.

[10] Mn_4: a) S. M. J. Aubin, N. R. Dilley, L. Pardi, J. Krzystek, M. W. Wemple, L.-C. Brunel, M. B. Maple, G. Christou, D. N. Hendrickson, *J. Am. Chem. Soc.* **1998**, *120*, 4991; b) J. Yoo, E. K. Brechin, A. Yamaguchi, M. Nakano, J. C. Huffman, A. L. Maniero, L.-C. Brunel, K. Awaga, H. Ishimoto, G. Christou, D. N. Hendrickson, *Inorg. Chem.* **2000**, *39*, 3615; c) E. K. Brechin, J. Yoo, M. Nakano, J. C. Huffman, D. N. Hendrickson, G. Christou, *Chem. Commun.* **1999**, 783; d) M. Wemple, D. M. Adams, K. S. Hagen, K. Folting, D. N. Hendrickson, G. Christou, *J. Chem. Soc. Chem. Commun.* **1995**, 1591; e) S. M. J. Aubin, M. W. Wemple, D. M. Adams, H.-L. Tsai, G. Christou, D. N. Hendrickson, *J. Am. Chem. Soc.* **1996**, *118*, 7746; $CrMn_6$: f) A. Scuiller, T. Mallah, M. Verdaguer, A. Nivorozkhin, J.-L. Tholence, P. Veillet, *New. J. Chem.* **1996**, *20*, 1; Mn_7: g) B. Pilawa, M. T. Kelemen, S. Wanka, A. Geisselmann, A. L. Barra, *Europhys. Lett.* **1998**, *43*, 7; Mn_{10}: h) A. L. Barra, A. Caneschi, D. Gatteschi, D. P. Goldberg, R. Sessoli, *J. Solid State Chem.* **1999**, *145*, 484.

[11] Mn_{12}: a) H. J. Eppley, H.-L. Tsai, N. De Vries, K. Folting, G. Christou, D. N. Hendrickson, *J. Am. Chem. Soc.* **1995**, *117*, 301; b) A. R. Schake, H.-L. Tsai, N. De Vries, R. J. Webb, K. Folting, D. N. Hendrickson, G. Christou, *J. Chem. Soc. Chem. Commun.* **1992**, 181; c) H.-L. Tsai, H. J. Eppley, N. De Vries, K. Folting, G. Christou, D. N. Hendrickson, *J. Chem. Soc. Chem. Commun.* **1994**, 1745; d) S. M. J. Aubin, S. Spagna, H. J. Eppley, R. E. Sager, G. Christou, D. N. Hendrickson, *Chem. Commun.* **1998**, 803; e) K. Takeda, K. Awaga, *Phys. Rev. B* **1997**, *56*, 14560; f) S. M. J. Aubin, Z. Sun, L. Pardi, J. Krzystek, K. Folting, L.-C. Brunel, A. L. Rheingold, G. Christou, D. N. Hendrickson, *Inorg. Chem.* **1999**, *38*, 5329; g) Z. Sun, D. Ruiz, E. Rumberger, C. D. Incarvito, K. Folting, A. L. Rheingold, G. Christou, D. N. Hendrickson, *Inorg. Chem.* **1998**, *37*, 4758; h) Z. Sun, D. Ruiz, N. R. Dilley, M. Soler, J. Ribas, K. Folting, M. B. Maple, G. Christou, D. N. Hendrickson, *Chem. Commun.* **1999**, 1973.

[12] V_4: S. L. Castro, Z. M. Sun, C. M. Grant, J. C. Bollinger, D. N. Hendrickson, G. Christou, *J. Am. Chem. Soc.* **1998**, *120*, 2365.

[13] a) J. Larionova, M. Gross, M. Pilkington, H. Andres, H. Stoeckli-Evans, H. U. Güdel, S. Decurtins, *Angew. Chem.* **2000**, *112*, 1667; *Angew. Chem. Int. Ed.* **2000**, *39*, 1605; b) G. Aromi, M. J. Knapp, J.-P.

Claude, J. C. Huffman, D. N. Hendrickson, G. Christou, *J. Am. Chem. Soc.* **1999**, *121*, 5489.
[14] A. L. Barra, D. Gatteschi, R. Sessoli, G. L. Abbati, A. Cornia, A. C. Fabretti, M. G. Uytterhoeven, *Angew. Chem* **1997**, *109*, 2423; *Angew. Chem. Int. Ed. Engl.* **1997**, *36*, 2329.
[15] A. Caneschi, A. Cornia, A. C. Fabretti, S. Foner, D. Gatteschi, R. Grandi, L. Schenetti, *Chem. Eur. J.* **1996**, *2*, 1379.
[16] a) A. Cornia, A. G. M. Jansen, M. Affronte, *Phys. Rev. B* **1999**, *60*, 12177; b) A. Cornia, M. Affronte, A. G. M. Jansen, G. L. Abbati, D. Gatteschi, *Angew. Chem* **1999**, *111*, 2409; *Angew. Chem. Int. Ed.* **1999**, *38*, 2264.
[17] a) A. Caneschi, A. Cornia, A. C. Fabretti, D. Gatteschi, *Angew. Chem.* **1999**, *111*, 1372; *Angew. Chem. Int. Ed.* **1999**, *38*, 1295; b) G. L. Abbati, A. Caneschi, A. Cornia, A. C. Fabretti, D. Gatteschi, *Inorg. Chim. Acta* **2000**, *297*, 291; c) G. L. Abbati, A. Cornia, A. C. Fabretti, W. Malavasi, L. Schenetti, A. Caneschi, D. Gatteschi, *Inorg. Chem.* **1997**, *36*, 6443; d) G. L. Abbati, A. Cornia, A. C. Fabretti, A. Caneschi, D. Gatteschi, *Inorg. Chem.* **1998**, *37*, 1430.
[18] F. Le Gall, F. Fabrizi de Biani, A. Caneschi, P. Cinelli, A. Cornia, A. C. Fabretti, D. Gatteschi, *Inorg. Chim. Acta* **1997**, *262*, 123.
[19] a) M. T. Andras, S. A. Duraj, A. F. Hepp, P. E. Fanwick, M. M. Bodnar, *J. Am. Chem. Soc.* **1992**, *114*, 786; b) P. Hodge, B. Piggott, *Chem. Commun.* **1998**, 1933.
[20] M. V. Capparelli, P. Hodge, B. Piggott, *Chem. Commun.* **1997**, 937.
[21] a) K. Dymock, G. J. Palenik, A. J. Carty, *J. Chem. Soc. Chem. Commun.* **1972**, 1218; b) W. Li, M. M. Olmstead, D. Miggins, R. H. Fish, *Inorg. Chem.* **1996**, *35*, 51; c) W. M. Cleaver, A. R. Barron, A. R. McGufey, S. G. Bott, *Polyhedron* **1994**, *13*, 2831; d) M. B. Hossain, M. A. F. Jalal, D. van der Helm, *J. Chem. Crystallogr.* **1998**, *28*, 57; e) D. J. Rose, Y. D. Chang, Q. Chen, P. B. Kettler, J. Zubieta, *Inorg. Chem.* **1995**, *34*, 3973; f) E. Hecht, *Z. Anorg. Allg. Chem.* **2000**, *626*, 1642; g) M. B. Power, W. M. Cleaver, A. W. Apblett, A. R. Barron, J. W. Ziller, *Polyhedron* **1992**, *11*, 477.
[22] R. R. Rakhimov, A. L. Wilkerson, G. B. Loutts, H. R. Ries, *J. Appl. Phys.* **1997**, *82*, 1970.
[23] a) A. Bencini, D. Gatteschi in *Transition Metal Chemistry*, *Vol. 8* (Eds.: G. A. Melson, B. N. Figgis), Marcel Dekker, New York, **1982**; b) B. R. McGarvey, *Transition Met. Chem.* **1966**, *3*, 89.
[24] O. Waldman, J. Schülein, R. Koch, P. Müller, I. Bernt, R. W. Saalfrank, H. P. Andres, H. U. Güdel, P. Allenspach, *Inorg. Chem.* **1999**, *38*, 5879.
[25] B. Silver, *Irreducible Tensor Methods—An Introduction for Chemists*, Academic Press, New York, **1976**, p. 2.
[26] a) I. Mirebeau, M. Hennion, H. Casalta, H. Andres, H. U. Güdel, A. V. Irodova, A. Caneschi, *Phys. Rev. Lett.* **1999**, *83*, 628; b) R. Caciuffo, G. Amoretti, A. Murani, R. Sessoli, A. Caneschi, D. Gatteschi, *Phys. Rev. Lett.* **1998**, *81*, 4744.
[27] a) J. M. Clemente, H. Andres, J. J. Borras-Almenar, E. Coronado, H. U. Güdel, M. Aebersold, G. Kearly, H. Buttner, M. Zolliker, *J. Am. Chem. Soc.* **1999**, *121*, 10021; b) H. Andres, J. M. Clemente, M. Aebersold, H. U. Güdel, E. Coronado, H. Büttner, G. Kearly, J. Melero, R. Burriel, *J. Am. Chem. Soc.* **1999**, *121*, 10028; c) H. Andres, M. Aebersold, H. U. Güdel, J. M. Clemente, E. Coronado, H. Büttner, G. Kearly, M. Zolliker, *Chem. Phys. Lett.* **1998**, *289*, 224.
[28] A. Bencini, D. Gatteschi, *EPR of Exchange Coupled Systems*, Springer, Berlin, **1990**.
[29] W. Wernsdorfer, A. Caneschi, R. Sessoli, D. Gatteschi, A. Cornia, V. Villar, C. Paulsen, *Phys. Rev. Lett.* **2000**, *84*, 2965.
[30] F. Neese, E. I. Solomon, *Inorg. Chem.* **1998**, *37*, 6568.
[31] A. Bencini, I. Ciofini, M. G. Uytterhoeven, *Inorg. Chim. Acta* **1998**, *274*, 90.
[32] L. Sorace, personal communication.
[33] a) G. Ingram, *Methods of Organic Elemental Microanalysis*, Chapman Hall, London, **1962**, p. 274; b) G. Ingram, *Methods of Organic Elemental Microanalysis*, Chapman Hall, London, **1962**, p. 176.
[34] A. I. Vogel, *Practical Organic Chemistry*, 3rd ed., Longmans, London, **1959**, p. 169.
[35] *SIR97*: *A New Program for Solving and Refining Crystal Structures*, IRMEC-CNR, Bari (Italy), **1997**.
[36] *SHELX-97*, University of Göttingen, Göttingen (Germany), **1997**.
[37] a) A. K. Hassan, L. A. Pardi, J. Krzystek, A. Sienkiewicz, P. Goy, M. Rohrer, L. C. Brunel, *J. Magn. Reson.* **2000**, *142*, 300; b) A. K. Hassan, A. L. Maniero, H. Van Tol, C. Saylor, L. C. Brunel, *Appl. Magn. Res.* **1999**, *16*, 299; c) G. Annino, M. Cassettari, M. Fittipaldi, I. Longo, M. Martinelli, C. A. Massa, L. A. Pardi, *J. Magn. Reson.* **2000**, *143*, 88.
[38] a) C. J. H. Jacobsen, E. Pedersen, J. Villadsen, H. Weihe, *Inorg. Chem.* **1993**, *32*, 1216; b) J. Glerup, H. Weihe, *Acta Chem. Scand.* **1991**, 444.
[39] a) *E04FCF*, *NAG Fortran Library Routine* (Mark 17), NAG Ltd, Oxford, **1996**; b) *ZHEEV*, *LAPACK driver routine (version 2.0)*, University of Tennessee, University of California Berkeley, NAG Ltd., Courant Institute, Argonne National Lab, Rice University, **1994**.
[40] *International Tables for X-ray Crystallography* (Ed.: T. Hahn), Reidel, Dordrecht, **1983**.
[41] D. Collison, A. K. Powell, *Inorg. Chem.* **1990**, *29*, 4735.

Received: September 29, 2000 [F2777]